

# Dual Adversarial Resilience for Collaborating Robust Underwater Image Enhancement and Perception

Zengxi Zhang<sup>1</sup>, Zhiying Jiang<sup>1</sup>, Zeru Shi<sup>1</sup>, Jinyuan Liu<sup>1</sup>, Risheng Liu<sup>1,2\*</sup>

<sup>1</sup>Dalian University of Technology, China

<sup>2</sup>Peng Cheng Laboratory, China

{cyouzoukyuu, zyjiang0630, shizeru77}@gmail.com, atlantis918@hotmail.com, rslu@dlut.edu.cn

## Abstract

Due to the uneven scattering and absorption of different light wavelengths in aquatic environments, underwater images suffer from low visibility and clear color deviations. With the advancement of autonomous underwater vehicles, extensive research has been conducted on learning-based underwater enhancement algorithms. These works can generate visually pleasing enhanced images and mitigate the adverse effects of degraded images on subsequent perception tasks. However, learning-based methods are susceptible to the inherent fragility of adversarial attacks, causing significant disruption in results. In this work, we introduce a collaborative adversarial resilience network, dubbed CARNet, for underwater image enhancement and subsequent detection tasks. Concretely, we first introduce an invertible network with strong perturbation-perceptual abilities to isolate attacks from underwater images, preventing interference with image enhancement and perceptual tasks. Furthermore, we propose a synchronized attack training strategy with both visual-driven and perception-driven attacks enabling the network to discern and remove various types of attacks. Additionally, we incorporate an attack pattern discriminator to heighten the robustness of the network against different attacks. Extensive experiments demonstrate that the proposed method outputs visually appealing enhancement images and perform averagely 6.71% higher detection mAP than state-of-the-art methods.

## Introduction

Due to the refraction of light and the reflection of fine particles underwater, wavelength-dependent light suffers from different attenuation degrees even at consistent depths, which greatly affects the visual effect of the image. Such distortions also detract from subsequent detection tasks. Therefore, underwater image enhancement has become one of the important computer vision tasks. With the development of underwater robots, a growing body of research (Liu et al. 2020c; Lin et al. 2021; Li et al. 2021; Fu et al. 2022; Huang et al. 2023) has employed deep learning to enhance underwater images in recent years. Among them, many (Liu et al. 2022b; Jiang et al. 2022; Zhang et al. 2023) also have utilized enhancement networks as preprocessing modules for detection tasks to improve prediction performance.

Despite the advancement of existing underwater image enhancement algorithms, the robustness of underwater en-

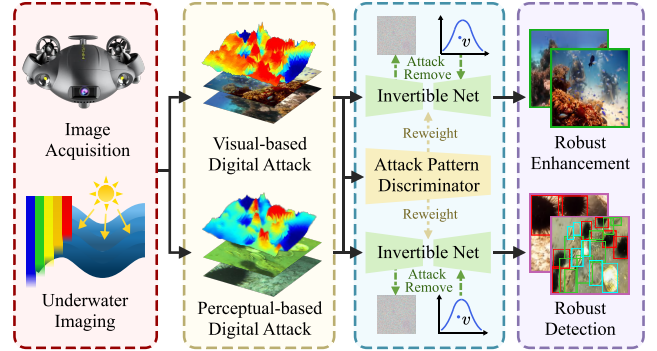


Figure 1: Overview of the underwater adversarial attack removal process. The proposed method can adaptively adjust the parameter weights of the network by discriminating the different attack patterns.

hancement networks has yet to be thoroughly studied. Even slight perturbations can significantly impact the predicted results of the network. In recent years, adversarial attacks have been applied to various computer vision tasks (Yu et al. 2022; Gui et al. 2023). These attacks not only disrupt the visual restoration effects of images but also significantly reduce the prediction performance of perception tasks.

In this paper, we consider adversarial attack as imperceptible high-frequency perturbations. Considering the advantages of invertible networks in high-frequency feature extraction, we propose a collaborative adversarial resilience network dubbed CARNet to enhance underwater images which suffer from different types of attacks, thus facilitating pleasing visual and detection results. Specifically, in the forward process, we transform the underwater image into latent components in different frequency domains and separate out the degradation factors of the underwater image. Subsequently, we reconstruct the clean enhanced image without attack in the inverse process. We further propose a synchronized attack training strategy for visual and perceptual attacks to enable the network to remove diverse attack types. Additionally, we propose an attack pattern discriminator that adjusts network parameters adaptively, optimizing its resilience to different attack forms.

In summary, our contributions are as follows:

\*Corresponding author

- We first introduce adversarial attacks to underwater tasks and propose a robust network for enhancement and detection tasks that counteracts the attack component in latent representations via an invertible framework.
- We propose a contrastive attack for underwater image enhancement and introduce a synchronized attack strategy so that the proposed network can simultaneously achieve robust underwater image enhancement and detection.
- We propose an attack pattern discriminator which learns different groups of convolution kernels and adjusts the weights of the network adaptively according to the input attack type to ensure reliable robustness.
- Extensive experiments on multiple underwater datasets demonstrate the effectiveness of our method.

## Related Work

### Underwater Image Enhancement

With the development of low-level image processing (Liu et al. 2012; Wu, Lin, and Zha 2019; Liu et al. 2020a, 2021b,a; Ma et al. 2022, 2023), underwater image enhancement has also received extensive attention. Existing traditional underwater enhancement methods can be classified into model-based methods and model-free methods. Model-based methods often incorporate domain knowledge as priors to assist in solving underwater enhancement problems, such as dark channel (Peng, Cao, and Cosman 2018) and red channel (Galdran et al. 2015). Model-free methods usually address the light attenuation phenomenon in underwater images by altering the pixel distribution. Examples of such methods include Retinex (Zhang et al. 2017) and MMLE (Zhang et al. 2022). There are also many deep learning-based approaches to improve image enhancement through data-driven networks (Liu et al. 2022b; Huang et al. 2023). In addition, there are many works that also use low-level visual tasks as upstream tasks to assist high-level visual tasks to improve the performance (Piao et al. 2019, 2020; Zhang et al. 2020; Liu et al. 2022a, 2023a,b). However, little work has been devoted to studying the vulnerability of underwater enhancement networks to adversarial attacks.

### Invertible Neural Network

Invertible neural networks (INNs) enable both forward and backward propagation within the same framework through the reversible mapping between the source domain  $x$  and target domain  $y$ . In recent years, INNs have been widely applied in computer vision tasks: (Xiao et al. 2020) proposed a reversible super-resolution network aiming to optimize the processes of upscaling and downscaling synchronously. (Jing et al. 2021) achieved image hiding by synchronously learning the processes of image concealing and revealing, with the secret image encoded into the wavelet domain. The purpose of this work is to leverage the encoding ability of invertible networks for high-frequency information to remove potential attacks in the input images.

### Adversarial Attack and Defense

Despite the outstanding representation capability of deep networks, it can also be damaged by slight perturbations.

In recent years, various attack methods have been proposed, which add visually imperceptible perturbations to input images, resulting in inaccurate predictions. Considering the linearity of neural networks, the Fast Gradient Sign Method (FGSM) (Goodfellow, Shlens, and Szegedy 2014) is first proposed to generate adversarial examples. I-FGCM (Kurakin, Goodfellow, and Bengio 2018) is introduced to iteratively update the perturbations within a limited attack range. Subsequently, (Madry et al. 2017) utilized local information of the network and employed a min-max optimization formulation. Adversarial attacks have been widely applied to various computer vision tasks. For low-level vision tasks, (Yin et al. 2018) first proposed a generic framework for adversarial attacks for image super-resolution. (Yu et al. 2022) conducted a comprehensive evaluation of the robustness in deraining and used efficient modules to construct networks against attacks. In the high-level vision domain, (Chen, Kung, and Chen 2021) adopted class-weighted adversarial training to uniformly enhance the robustness of the detection model. (Dong, Wei, and Lin 2022) proposed a robust detector based on adversarial-aware convolutions. Attacks designed for low-level and high-level vision tasks have significant differences. Unfortunately, there is no network yet that can defend against both vision-driven and perception-driven attacks simultaneously.

## Method

By incorporating visually imperceptible perturbations  $\delta$  into underwater images, the performance of deep learning tasks can be significantly disrupted. Such perturbations are referred to as underwater adversarial attacks, which can be depicted as follows:

$$\delta = \arg \max_{\delta} \mathcal{M}(\mathbf{r}, f(\mathbf{x} + \delta | \omega)), \quad (1)$$

where  $\mathbf{x}$  represents the underwater image,  $f(\cdot | \omega)$  denotes the deep network designed for underwater tasks, which is parameterized by  $\omega$ .  $\mathcal{M}$  means the metric for measuring network performance.  $\mathbf{r}$  denotes the task-dependent reference information. We hope that by adding perturbation, which maximizes the difference between outputs of the network from the attacked image and the reference. Widely used PGD (Madry et al. 2017) was employed to obtain perturbations iteratively, which can be represented as:

$$\delta^{t+1} = \delta^t + \alpha \text{sgn}(\nabla_{\delta} \mathcal{M}), \quad (2)$$

where  $\text{sgn}$  aims to extract the gradient  $\nabla_{\delta}$ .  $\alpha$  represents the step size of each iteration.  $\delta_0$  is sampled from a uniform distribution and then iteratively updates adversarial attacks. Notably,  $\delta^{t+1}$  is clipped into  $(-\epsilon, \epsilon)$  after each iteration to ensure that the disturbance will not cause obvious visual damage to the input image.  $\epsilon$  is a constant value.

## Overall Invertible Framework

As for the underwater image enhancement, we denote the attacked underwater image as  $y$  and the clean restored image as  $z$ . The degradation factor caused by the physical underwater imaging model (Drews et al. 2013) is represented

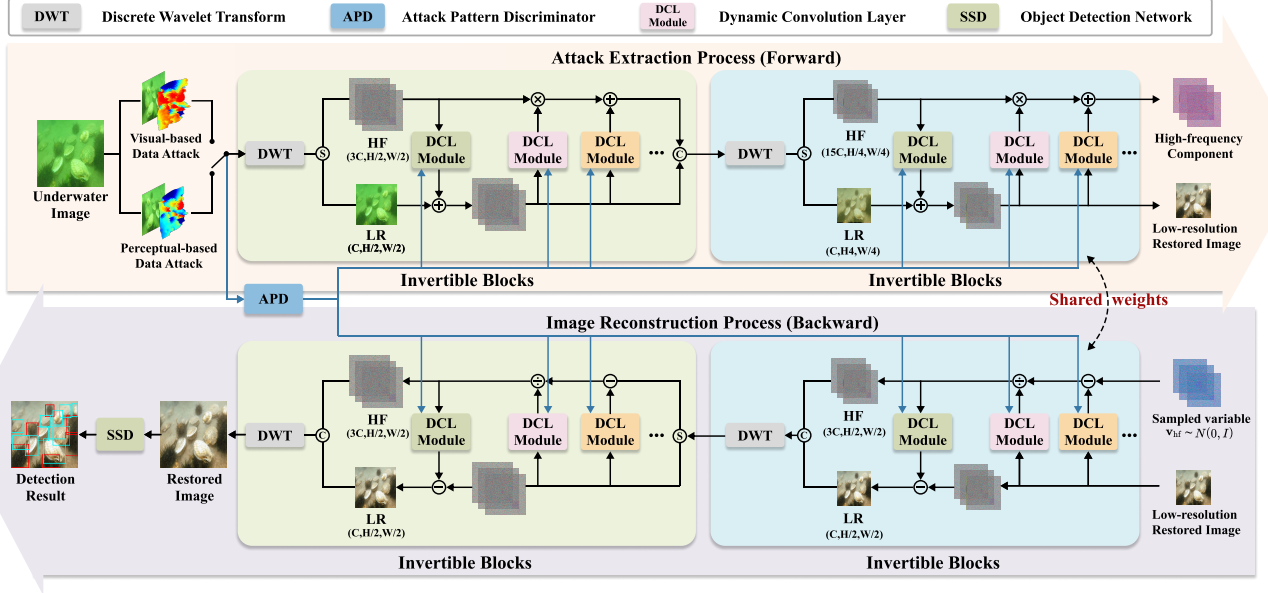


Figure 2: Workflow of the proposed CARNet. In the forward process, the attacked underwater image is transformed into low-resolution image and latent high-frequency component. In the backward process, the high-frequency component is replaced with sampled distribution which is only embedded with clean details to reconstruct enhanced images without attacks.

as  $\varphi$ . Therefore, the attack on an underwater image can be expressed as:  $p(\mathbf{y}) = p(\mathbf{z}, \varphi, \delta) = p(\mathbf{z})p(\varphi, \delta|\mathbf{z})$ . It is obvious that the attacked underwater image contains both potential clean information and degradation information which resulted from physical and digital attacks.

The workflow of our method is shown in Fig. 2. Instead of directly decoupling the clean and degradation information, we aim to separate the low-resolution and high-frequency components of  $\mathbf{y}$  by employing wavelet transform and a set of invertible operations. Considering that the invertible network maintains information integrity (Liu et al. 2021c), we make the first three channels of latent components fit to the clean image after downsampling and fully encode high-frequency information into the remaining channels. Therefore, in the output of the forward process, the features are explicitly decomposed into the low-resolution restored image  $\mathbf{x}_{lr}$  and the high-frequency component  $\mathbf{x}_{hf}$  containing the degradation information, which is expressed as follows:

$$p(\mathbf{y}) = p(\mathbf{x}_{lr}, \mathbf{x}_{hf}, \varphi, \delta) = p(\mathbf{x}_{lr})p(\mathbf{x}_{hf}, \varphi, \delta|\mathbf{x}_{lr}). \quad (3)$$

During the backward process, we discard all degradation information and reconstruct a clean image from the low-resolution components. However, the high-frequency components obtained by the invertible network contain not only the degradation information but also a part of the clean image. Since it is difficult to effectively decouple them, during the backward process, we replace  $\mathbf{x}_{hf}$  with the sampled  $\mathbf{v}_{hf} \sim N(0, I)$  and combine with  $\mathbf{x}_{lr}$  to reconstruct a clean image  $\mathbf{z}$  without degradation information. Under the bilateral constraint, the clean details of  $\mathbf{x}_{hf}$  are then embedded into the latent variable  $\mathbf{v}_{hf}$  to achieve a good attack removal effect. The constraints on the forward and backward process

are illustrated as follows:

$$\begin{aligned} \mathcal{L}_{\text{forw}} &= \frac{1}{M} \sum_{i=1}^M \|f_+(\mathbf{y})_{lr} - \mathbf{z}_{lr}\|_1, \\ \mathcal{L}_{\text{back}} &= \frac{1}{N} \sum_{i=1}^N \|f_-(f_+(\mathbf{y})_{lr}, \mathbf{v}_{hf}) - \mathbf{z}\|_1, \end{aligned} \quad (4)$$

where  $f_+$  and  $f_-$  denote the forward and backward process.  $\mathbf{z}_{lr}$  means the low resolution version of  $\mathbf{z}$ , which is conducted by bicubic transformation.  $M$  and  $N$  represent the number of pixels. The SSD detector (Liu et al. 2016) is conducted after the clean image is generated to get detection results. The constraint on object detection is as follows:

$$\mathcal{L}_{\text{det}} = \mathcal{L}_{\text{cls}} + \mathcal{L}_{\text{loc}}, \quad (5)$$

where  $\mathcal{L}_{\text{cls}}$  denotes the classification loss, which is designed to minimize the discrepancy between the predicted and ground truth categories.  $\mathcal{L}_{\text{loc}}$  is the localization loss for reducing the difference between the predicted and label boxes.

### Synchronized Attack Training Strategy

Adversarial attacks on underwater images can be divided into two types: Vision-driven attack  $\delta_v$  and perception-driven attack  $\delta_p$ . The main difference between them is the design of  $M$  from Eq. (1). Vision-driven adversarial attacks usually employ pixel-level evaluation metrics for underwater image enhancement, such as  $l_1$  norm. Perception-driven adversarial attacks usually use metrics for corresponding downstream tasks, such as  $\mathcal{L}_{\text{cls}}$  and  $\mathcal{L}_{\text{loc}}$ . In order to fortify the proposed network against diverse attacks, we propose the Synchronized Attack Training Strategy, which is illustrated in Alg. 1. Notably, we introduce the contrastive principle

into the metric  $\mathcal{M}$  from Eq. (2) and propose a contrastive attack as vision-driven attacks for underwater image enhancement, which enforces the attacked enhanced results closer to the underwater images and far away from the reference images. The metric for the proposed attack is expressed as:

$$\mathcal{M}_{CA} = \|f(\mathbf{x} + \delta \mid \omega) - \mathbf{z}\|_1 - \|f(\mathbf{x} + \delta \mid \omega) - \mathbf{x}\|_1, \quad (6)$$

where attacked underwater images  $\mathbf{x}$  and clean reference images  $\mathbf{z}$  denote positive and negative samples, respectively. Class Weight Attack (CWA) (Chen, Kung, and Chen 2021) is introduced as the perception-driven attack for underwater object detection task.

---

**Algorithm 1:** Synchronized Attack Training Strategy

---

**Require:** maximum iterations  $N$ ; step size  $S$ ; batch size  $m$  ( $m$  must be an even number); The proposed network  $f$  with the parameter  $\omega$ .

- 1: **for** iter = 1 :  $N$  **do**
- 2:   Sample underwater images  $X \leftarrow [x^1, x^2 \dots x^m]$ ;
- 3:   Split  $X$  into  $X^1 \leftarrow [x^1, x^2 \dots x^{m/2}]$  and  $X^2 \leftarrow [x^{m/2+1}, x^{m/2+2} \dots x^m]$ ;
- 4:   initial  $\delta_v^0$  and  $\delta_p^0$  from the distribution  $U \sim (-\epsilon, \epsilon)$ ;
- 5:   **for** t = 1 :  $S$  **do**
- 6:      $\delta_v^{t+1} \leftarrow \delta_v^t + \alpha \operatorname{sgn}(\nabla_{\delta_v} \mathcal{M}_{CA})$ ;
- 7:      $\delta_p^{t+1} \leftarrow \delta_p^t + \alpha \operatorname{sgn}(\nabla_{\delta_p} \mathcal{M}_{CWA})$ ;
- 8:   **end for**
- 9:    $X^1 \leftarrow X^1 + \delta_v^S, X^2 \leftarrow X^2 + \delta_p^S$ ;
- 10:   Merge  $X^1$  and  $X^2$  into  $X$ ;
- 11:   Updating parameters  $\omega$  by supervised training.
- 12: **end for**

---

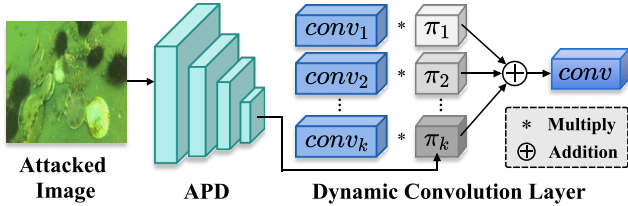


Figure 3: The reweighting process from Attack Pattern Discriminator to Dynamic Convolution Layer.

### Attack Pattern Discriminator

Different types of attacks show diametrically opposite effects on images. Vision-driven Adversarial attacks often have limited impact on detection tasks, and vice versa. Therefore, it is difficult for traditional networks with fixed parameters to discern and remove both types of attacks. Inspired by (Chen et al. 2020), instead of employing convolution blocks to learn common features of underwater images under different attacks, we introduce Dynamic Convolution Layer (DCL) in the invertible network, which aggregates multiple parallel convolution kernels dynamically based upon attention weights. Rather than only considering the similarity between visual-driven and perception-driven

attacks, the difference between the two types of aggression is additionally learned by proposing an Attack Pattern Discriminator, which generates input-dependent weights for DCL by identifying the attack type of an input image. The structure of APD is Resnet18 (He et al. 2016). The process of Attack Pattern Discriminator reweight DCL is shown in Fig. 3. Since APD is also attacked in the training process, we employ Online Triplet Constraint (Schroff, Kalenichenko, and Philbin 2015) to APD, which is shown as follows:

$$\mathcal{L}_{APD} = \sum_{i=1}^{N_T} (JS(APD(x_i^a), APD(x_i^p)) - JS(APD(x_i^a), APD(x_i^n)) + \gamma)_+, \quad (7)$$

where  $JS$  represents Jensen-Shannon divergence (Lin 1991) of two distributions.  $x_i^p$  and  $x_i^n$  represents the corresponding positive and negative pairs of  $x_i^a$ ,  $\gamma$  is the margin that is enforced between  $x_i^a$  and  $x_i^p$ .  $M$  denotes the number of triplets. Therefore, the whole constraint during the training process can be expressed as:

$$\mathcal{L}_{train} = \lambda_1 \mathcal{L}_{forw} + \lambda_2 \mathcal{L}_{back} + \lambda_3 \mathcal{L}_{det} + \lambda_4 \mathcal{L}_{APD}. \quad (8)$$

### Experiments

In this section, we evaluate the effectiveness of our method on underwater enhancement and detection tasks through quantitative and qualitative experiments. Specifically, widely used datasets UIEBD (Li et al. 2019) and UCCS (Liu et al. 2020b) are used to assess the performance of our method on underwater enhancement tasks. Underwater Color Image Quality Evaluation (UCIQE) (Yang and Sowmya 2015), Underwater Image Quality Measurement (UIQM) (Panetta, Gao, and Agaian 2015), Underwater Absorption and Scattering Characteristics (CCF) (Wang et al. 2018) and Self-adaptive Hyper Network Architecture (HIQE) (Su et al. 2020) are employed as unsupervised image quality evaluation metrics. Additionally, Peak Signal to Noise Ratio (PSNR) and Structural Similarity (SSIM) (Wang et al. 2004) are used as full-reference metrics on the UIEBD dataset with reference images. Higher values of these metrics indicate better image quality.

ChinaMM (Liu et al. 2020b), Aquarium (Prytula 2020), and UTDAC2020 (Chen et al. 2022) datasets are used for evaluating our method on underwater object detection tasks. The mean Average Precision (mAP) is adopted as the evaluation metric to measure the accuracy of the current method. Widely used object detection adversarial attacks, including traditional attacks  $A_{cls}$ ,  $A_{loc}$ , and well-crafted attacks CWA (Chen, Kung, and Chen 2021), DAG (Xie et al. 2017) are employed to comprehensively evaluate the robustness of our method. For fair comparisons, we select recent learning-based enhancement methods FGAN (Islam, Xia, and Sattar 2020), DLIFM (Chen et al. 2021), TOPAL (Jiang et al. 2022), CWR (Han et al. 2022), and TACL (Liu et al. 2022b), which use traditional supervised training without providing additional prior information, as our comparative methods. Additionally, we subject each method to the same adversarial training strategy to demonstrate the robustness of our network in an intuitive manner.



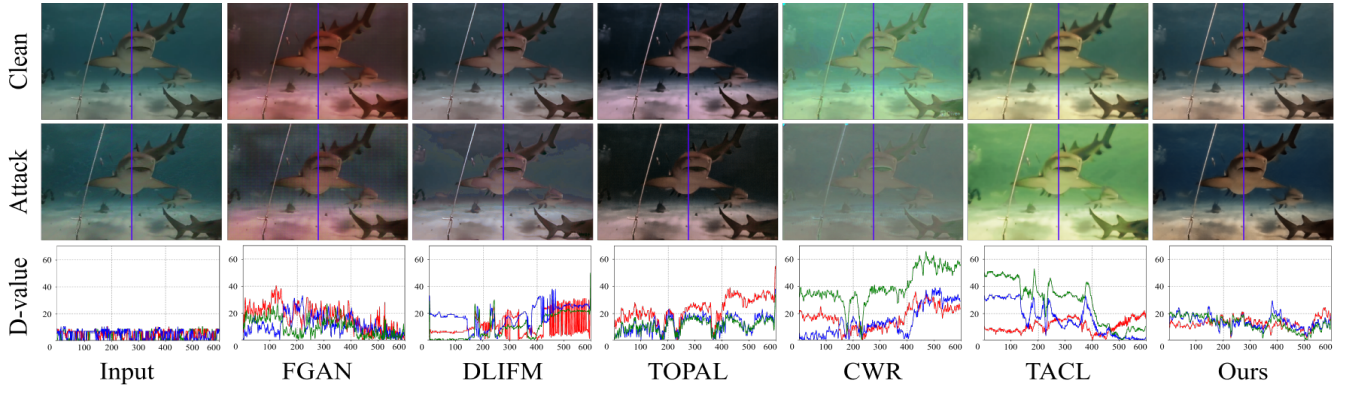


Figure 4: Enhancement results on UIEBD dataset. The line graph represents the image difference between the clean image and the attack image after enhancement. Smaller differences indicate better robustness.

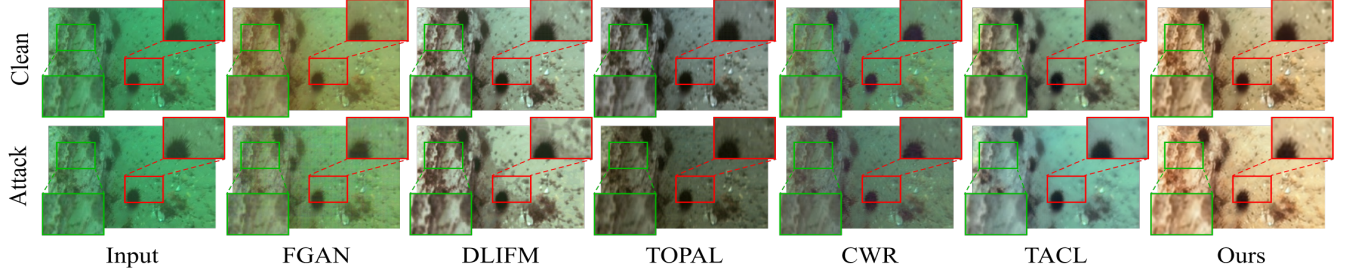


Figure 5: Enhancement results on UCCS dataset.

Method	UIEBD						UCCS			
	UCIQE(↑)	UIQM(↑)	CCF(↑)	HIQA(↑)	PSNR(↑)	SSIM(↑)	UCIQE(↑)	UIQM(↑)	CCF(↑)	HIQA(↑)
FGAN	0.5457	3.1130	14.6655	0.2954	15.7601	0.6731	<b>0.5235</b>	0.4920	<b>34.6400</b>	0.3071
DLIFM	<u>0.5742</u>	<u>3.0996</u>	<u>34.1644</u>	0.3069	<b>17.2531</b>	<b>0.7824</b>	0.5103	<u>3.0314</u>	19.2414	<u>0.3228</u>
TOPAL	0.5644	2.6111	20.7014	0.2677	16.9008	0.6939	0.4740	2.6549	19.2167	0.2903
CWR	0.4782	1.4180	12.7102	<u>0.3164</u>	15.8725	0.7430	0.4922	2.7220	20.1460	0.3133
TACL	0.5474	2.1029	16.1894	0.2841	16.9635	0.7637	0.5026	2.7101	22.5207	0.2826
Ours	<b>0.5756</b>	<b>3.1814</b>	<b>36.1170</b>	<b>0.3199</b>	<u>16.9858</u>	<u>0.7680</u>	<u>0.5190</u>	<b>3.2081</b>	<u>21.5031</u>	<b>0.3374</b>

Table 1: Quantitative comparison for underwater image enhancement without adversarial attacks in terms of UCIQE(↑), UIQM(↑), CCF(↑), HIQA(↑), PSNR(↑) and SSIM(↑). ↑ denotes that large values means better results. The best and second results are marked in **bold** and underline.

Method	UIEBD						UCCS			
	UCIQE(↑)	UIQM(↑)	CCF(↑)	HIQA(↑)	PSNR(↑)	SSIM(↑)	UCIQE(↑)	UIQM(↑)	CCF(↑)	HIQA(↑)
FGAN	0.5390	<u>3.1750</u>	14.8937	0.2582	15.3797	0.6305	0.4851	0.5399	<b>30.0805</b>	0.2449
DLIFM	<u>0.5693</u>	2.8989	<u>33.5000</u>	0.3024	<u>16.6299</u>	<u>0.7111</u>	0.5074	3.3010	17.2121	<u>0.3258</u>
TOPAL	0.5285	3.1592	18.3976	0.2888	15.4115	0.5758	0.4659	2.9198	17.6328	0.2915
CWR	0.4674	1.1390	10.2276	<u>0.3100</u>	13.1063	0.5902	0.4922	2.7220	20.3100	0.3252
TACL	0.5251	1.7404	14.9788	0.2810	15.7862	0.7031	<u>0.5106</u>	<u>3.3805</u>	16.1894	0.2761
Ours	<b>0.5829</b>	<b>3.3715</b>	<b>35.2089</b>	<b>0.3139</b>	<b>16.6385</b>	<b>0.7167</b>	<b>0.5131</b>	<b>3.6918</b>	<u>21.5287</u>	<b>0.3440</b>

Table 2: Quantitative comparison for underwater image enhancement under adversarial attacks.

## Implement Details

The proposed network is implemented in Pytorch and trained on NVIDIA RTX 2080 GPU. We first pre-train the enhancement part for 300,000 iterations and the detection

part for 120000 iterations separately. UIEBD is used as the training dataset for image enhancement. ChinaMM, Aquarium and UTDAC2020 are used as the training dataset for object detection, respectively. Subsequently, we jointly train

Method	ChinaMM					Aquarium					UTDAC2020				
	Clean	A <sub>cls</sub>	A <sub>loc</sub>	CWT	DAG	Clean	A <sub>cls</sub>	A <sub>loc</sub>	CWT	DAG	Clean	A <sub>cls</sub>	A <sub>loc</sub>	CWT	DAG
SSD	<b>91.36</b>	10.70	13.46	9.90	42.63	<b>55.42</b>	2.61	2.84	0.97	15.76	<b>67.30</b>	4.03	5.91	0.22	7.94
SSD-AT	57.42	38.74	44.18	40.28	46.67	26.80	16.36	24.04	19.92	21.20	16.15	9.74	13.98	14.33	11.85
DLIFM	65.86	43.62	44.31	49.63	52.16	43.08	16.19	17.12	15.20	32.24	22.34	13.22	14.52	16.67	18.26
FGAN	76.58	38.01	38.92	42.27	46.51	46.26	17.52	24.00	18.21	23.25	26.17	13.51	13.98	16.86	19.90
TOPAL	79.03	72.52	67.96	62.40	69.16	47.54	24.53	27.41	25.02	31.86	26.34	14.96	15.13	17.92	20.32
CWR	80.64	72.20	72.92	68.62	74.52	46.51	21.17	23.68	22.77	29.81	28.52	14.82	15.43	16.56	18.66
TACL	82.21	<u>76.69</u>	<u>78.14</u>	<u>72.66</u>	<u>79.26</u>	47.36	<u>26.10</u>	<u>29.44</u>	<u>27.12</u>	<u>36.28</u>	31.17	<u>16.28</u>	<u>16.92</u>	<u>18.00</u>	<u>21.26</u>
Ours	<u>90.30</u>	<b>84.61</b>	<b>84.83</b>	<b>81.14</b>	<b>89.85</b>	<u>51.79</u>	<b>32.63</b>	<b>39.15</b>	<b>32.01</b>	<b>45.26</b>	<u>44.32</u>	<b>18.86</b>	<b>18.37</b>	<b>21.58</b>	<b>24.97</b>

Table 3: Quantitative comparison for underwater object detection in terms of mAP( $\uparrow$ ).

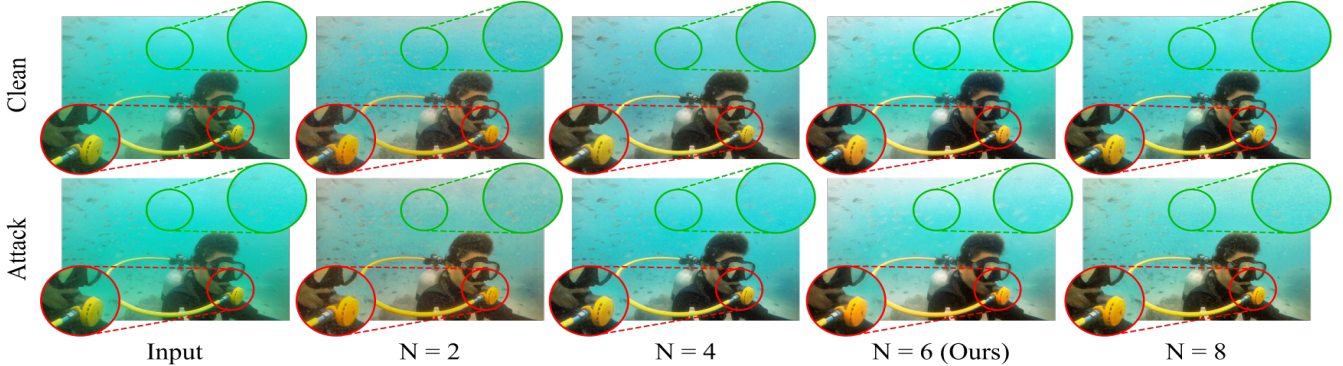


Figure 6: Enhancement results of ablation study on the number of Attack Removing Blocks.

for 200,000 iterations on image enhancement and object detection tasks by using the proposed training strategy. During the training process, SGD is employed as the optimizer for our network, with the learning rate set to  $1e-4$ .  $\lambda_1$ ,  $\lambda_2$ ,  $\lambda_3$ ,  $\lambda_4$  is set to 2, 0.1, 1, 5 respectively.

### Qualitative Results

We first evaluate the performance of our method on the underwater image enhancement task. Fig. 4 shows the performance of our method on the UIEBD dataset. The results in the first and second rows represent the enhancement results obtained by all methods without and with adversarial attacks, respectively. From the results without attacks, CWR and TACL show limited enhancement effects on underwater images. FGAN produces additional artifacts which make the result deviate from the original color. While TOPAL restores a good color appearance to the image, it suffers from dark reflection. After introducing adversarial attacks, the enhancement effects of CWR and TACL are further weakened after being attacked. DLIFM is affected by local over-enhancement, which destroys the overall structural appearance of the image. FGAN is disturbed by obvious noise, resulting in artifacts and unnatural colors. In contrast, only the proposed method generates relatively satisfactory images both unattacked and attacked. We further evaluate whether the enhanced results from the unattacked and the attacked inputs have appearance consistency. The line chart in the third row represents the absolute value of the intensity difference between the unattacked and the attacked enhanced

image on the RGB channels. It can be clearly seen that our image variance is significantly smaller than other methods, which proves the robustness of the proposed method.

Fig. 5 shows the enhancement effect of the proposed method on the UCCS dataset. While FGAN, DLIFM and CWR show some improvement in image contrast, they lack effectiveness in fully eliminating color casts and artifacts. After being attacked, they show more obvious color artifacts. TOPAL suffers from low saturation, which is exacerbated after introducing attacks. Adversarial training makes TACL lose the details of the content during the enhancement process, resulting in blurred enhanced images. In contrast, our images not only generate bright reflections but also recover richer detail information.

### Quantitative Results

Table 1 presents the quantitative results of the proposed method without attacks. On the UIEBD dataset, our method outperforms existing methods in all metrics except PSNR and SSIM, where they are slightly behind DLIFM. On the UCCS dataset, our method achieved the best performance in UIQM and HIQA, and is only lower than DLIFM in UCIQE and CCF. Table 2 shows the quantitative results under attacks. It can be clearly seen that the advantage of our method is further enhanced. On the UIEBD dataset, compared with the clean version, it surpasses DLIFM in both PSNR and SSIM, and the gaps with the second highest metrics (UCIQE, UIQM, and HIQA) increased from 0.24%, 2.19%, and 1.09% to 2.38%, 6.18%, and 1.25%, respec-

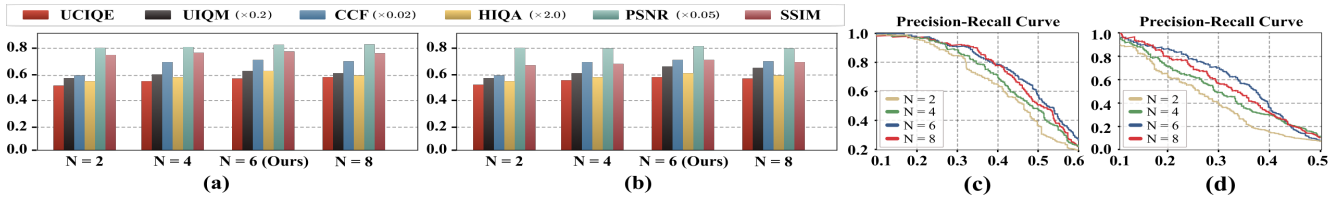


Figure 7: Quantitative results of ablation study on the number of Attack Removing Blocks.

tively. On the UCCS dataset, only CCF remained lower than FGAN, while all other metrics surpassed other methods.

Table 3 demonstrates the quantitative results of the proposed method on three detection datasets. SSD represents the detection results without using any enhancement network for joint training and without adversarial training. SSD-AT is the adversarial-trained version of SSD. It can be observed that when no adversarial training is conducted, the mean average precision (mAP) on clean images is higher than all existing methods. However, the mAP drops significantly once any attack is applied. Compared with existing methods, the proposed method shows the least difference with pure SSD in test performance on clean images. Meanwhile, the precision on the attacked underwayer images is significantly higher than all other methods.

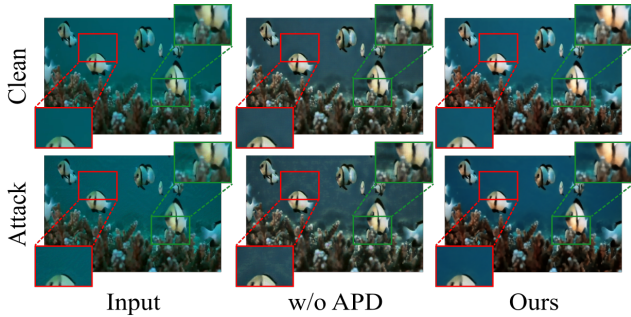


Figure 8: Enhancement results of ablation study on the Attack Pattern Discriminator.

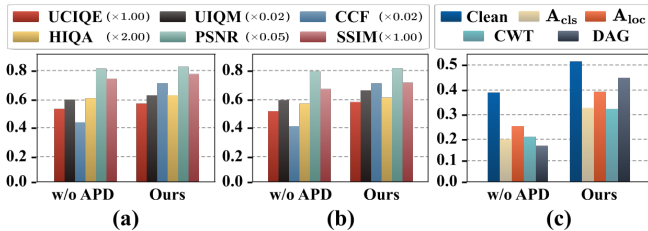


Figure 9: Quantitative results of ablation study on the Attack Pattern Discriminator.

## Ablation Study

**Study on Number of Invertible Blocks:** The proposed method consists of multiple invertible blocks. We explored the influence of the number of Invertible Blocks for our method. The visualization of enhancement results is shown in Fig. 6. It is evident that the enhancement results when N

= 2 shows a certain extent of color casting. When N = 8, the introduction of the attack introduces additional noise interference in the enhanced image, especially noticeable in the content within the green box. Compared with N = 4, which produces a relatively vivid appearance, N = 6 substantially radiance and contrast of the scene. The quantitative results are shown in Fig. 7, where (a) and (b) represent the enhancement results without and with attack. When testing on clean images, N = 6 performs slightly lower than N = 8 in PSNR, while all other metrics reach their optimum. After being attacked, N = 6 outperforms all other configurations in all metrics. (c) and (d) denote the detection comparison on clean and attacked images, in which the detections result when N = 6 is evidently better than other results. Therefore, we ultimately set N = 6 in our method.

**Study on Attack Pattern Discriminator:** To verify the performance of the Attack Pattern Discriminator, we investigated the enhancement and detection performance of the network without APD. The qualitative results for underwater image enhancement are shown in Fig. 8. It can be clearly seen that the enhancement performance is significantly affected by attacks when APD is not employed. Especially in the red box, the background in the distance is heavily disturbed by noise. Compared with the unpleasing results, the proposed method not only mitigates the interference of attacks to a greater extent but also attenuates the unwanted blue color attributed to light absorption and scattering. Fig. 9 presents the quantitative results of our method in image enhancement and object detection. (a) and (b) denote the evaluation on enhancement results with unattacked and attacked images. (c) shows the comparison on detection results. The proposed method exceeds the method without APD in all metrics, which demonstrate the superiority of APD.

## Conclusion

This work proposes an precision and robustness collaborative network to enhance underwater images against various attacks, resulting in improved visual and detection predictions. In the forward process, underwater images are transformed into latent components across different frequency domains for isolating degradation factors. Then we reconstruct enhanced images without attacks in the backward process. We also employ an adversarial training strategy for both visual and perceptual attacks, enabling the network to remove multiple attack types. Additionally, we introduce the Attack Pattern Discriminator to ensure a reliable robustness. Experimental results illustrated that the proposed method can achieve robust enhancement and detection results.



## References

- Chen, L.; Zhou, F.; Wang, S.; Dong, J.; Li, N.; Ma, H.; Wang, X.; and Zhou, H. 2022. SWIPENET: Object detection in noisy underwater scenes. *Pattern Recognition*, 132: 108926.
- Chen, P.-C.; Kung, B.-H.; and Chen, J.-C. 2021. Class-aware robust adversarial training for object detection. In *Proceedings of the IEEE/CVF Conference on Computer Vision and Pattern Recognition*, 10420–10429.
- Chen, X.; Zhang, P.; Quan, L.; Yi, C.; and Lu, C. 2021. Underwater image enhancement based on deep learning and image formation model. *arXiv preprint arXiv:2101.00991*.
- Chen, Y.; Dai, X.; Liu, M.; Chen, D.; Yuan, L.; and Liu, Z. 2020. Dynamic Convolution: Attention Over Convolution Kernels. In *Proceedings of the IEEE/CVF Conference on Computer Vision and Pattern Recognition (CVPR)*.
- Dong, Z.; Wei, P.; and Lin, L. 2022. Adversarially-aware robust object detector. In *European Conference on Computer Vision*, 297–313. Springer.
- Drews, P.; Nascimento, E.; Moraes, F.; Botelho, S.; and Campos, M. 2013. Transmission estimation in underwater single images. In *Proceedings of the IEEE international conference on computer vision workshops*, 825–830.
- Fu, Z.; Lin, H.; Yang, Y.; Chai, S.; Sun, L.; Huang, Y.; and Ding, X. 2022. Unsupervised Underwater Image Restoration: From a Homology Perspective. In *AAAI Conference on Artificial Intelligence (AAAI)*, volume 36, 643–651.
- Galdran, A.; Pardo, D.; Picón, A.; and Alvarez-Gila, A. 2015. Automatic red-channel underwater image restoration. *Journal of Visual Communication and Image Representation*, 26: 132–145.
- Goodfellow, I. J.; Shlens, J.; and Szegedy, C. 2014. Explaining and harnessing adversarial examples. *arXiv preprint arXiv:1412.6572*.
- Gui, J.; Cong, X.; Peng, C.; Tang, Y. Y.; and Kwok, J. T.-Y. 2023. Adversarial Attack and Defense for Dehazing Networks. *arXiv preprint arXiv:2303.17255*.
- Han, J.; Shoeiby, M.; Malthus, T.; Botha, E.; Anstee, J.; Anwar, S.; Wei, R.; Armin, M. A.; Li, H.; and Petersson, L. 2022. Underwater image restoration via contrastive learning and a real-world dataset. *Remote Sensing*, 14(17): 4297.
- He, K.; Zhang, X.; Ren, S.; and Sun, J. 2016. Deep residual learning for image recognition. In *Proceedings of the IEEE conference on computer vision and pattern recognition*, 770–778.
- Huang, S.; Wang, K.; Liu, H.; Chen, J.; and Li, Y. 2023. Contrastive semi-supervised learning for underwater image restoration via reliable bank. In *Proceedings of the IEEE/CVF Conference on Computer Vision and Pattern Recognition*, 18145–18155.
- Islam, M. J.; Xia, Y.; and Sattar, J. 2020. Fast underwater image enhancement for improved visual perception. *IEEE Robotics and Automation Letters*, 5(2): 3227–3234.
- Jiang, Z.; Li, Z.; Yang, S.; Fan, X.; and Liu, R. 2022. Target Oriented Perceptual Adversarial Fusion Network for Underwater Image Enhancement. *IEEE Transactions on Circuits and Systems for Video Technology*.
- Jing, J.; Deng, X.; Xu, M.; Wang, J.; and Guan, Z. 2021. HiNet: deep image hiding by invertible network. In *Proceedings of the IEEE/CVF international conference on computer vision*, 4733–4742.
- Kurakin, A.; Goodfellow, I. J.; and Bengio, S. 2018. Adversarial examples in the physical world. In *Artificial intelligence safety and security*, 99–112. Chapman and Hall/CRC.
- Li, C.; Anwar, S.; Hou, J.; Cong, R.; Guo, C.; and Ren, W. 2021. Underwater image enhancement via medium transmission-guided multi-color space embedding. *IEEE Transactions on Image Processing*, 30: 4985–5000.
- Li, C.; Guo, C.; Ren, W.; Cong, R.; Hou, J.; Kwong, S.; and Tao, D. 2019. An underwater image enhancement benchmark dataset and beyond. *IEEE Transactions on Image Processing*, 29: 4376–4389.
- Lin, J. 1991. Divergence measures based on the Shannon entropy. *IEEE Transactions on Information theory*, 37(1): 145–151.
- Lin, R.; Liu, J.; Liu, R.; and Fan, X. 2021. Global structure-guided learning framework for underwater image enhancement. *The Visual Computer*, 1–16.
- Liu, J.; Fan, X.; Huang, Z.; Wu, G.; Liu, R.; Zhong, W.; and Luo, Z. 2022a. Target-aware dual adversarial learning and a multi-scenario multi-modality benchmark to fuse infrared and visible for object detection. In *Proceedings of the IEEE/CVF Conference on Computer Vision and Pattern Recognition*, 5802–5811.
- Liu, J.; Fan, X.; Jiang, J.; Liu, R.; and Luo, Z. 2021a. Learning a deep multi-scale feature ensemble and an edge-attention guidance for image fusion. *IEEE Transactions on Circuits and Systems for Video Technology*, 32(1): 105–119.
- Liu, J.; Liu, Z.; Wu, G.; Ma, L.; Liu, R.; Zhong, W.; Luo, Z.; and Fan, X. 2023a. Multi-interactive Feature Learning and a Full-time Multi-modality Benchmark for Image Fusion and Segmentation. *arXiv preprint arXiv:2308.02097*.
- Liu, J.; Wu, G.; Luan, J.; Jiang, Z.; Liu, R.; and Fan, X. 2023b. HoLoCo: Holistic and local contrastive learning network for multi-exposure image fusion. *Information Fusion*, 95: 237–249.
- Liu, R.; Fan, X.; Zhu, M.; Hou, M.; and Luo, Z. 2020a. Real-world underwater enhancement: Challenges, benchmarks, and solutions under natural light. *IEEE transactions on circuits and systems for video technology*, 30(12): 4861–4875.
- Liu, R.; Fan, X.; Zhu, M.; Hou, M.; and Luo, Z. 2020b. Real-world underwater enhancement: Challenges, benchmarks, and solutions under natural light. *IEEE Transactions on Circuits and Systems for Video Technology*, 30(12): 4861–4875.
- Liu, R.; Jiang, Z.; Yang, S.; and Fan, X. 2022b. Twin adversarial contrastive learning for underwater image enhancement and beyond. *IEEE Transactions on Image Processing*, 31: 4922–4936.
- Liu, R.; Li, S.; Liu, J.; Ma, L.; Fan, X.; and Luo, Z. 2020c. Learning hadamard-product-propagation for image dehazing and beyond. *IEEE Transactions on Circuits and Systems for Video Technology*, 31(4): 1366–1379.

- Liu, R.; Lin, Z.; De la Torre, F.; and Su, Z. 2012. Fixed-rank representation for unsupervised visual learning. In *2012 IEEE conference on computer vision and pattern recognition*, 598–605. IEEE.
- Liu, R.; Ma, L.; Zhang, J.; Fan, X.; and Luo, Z. 2021b. Retinex-inspired unrolling with cooperative prior architecture search for low-light image enhancement. In *Proceedings of the IEEE/CVF Conference on Computer Vision and Pattern Recognition*, 10561–10570.
- Liu, W.; Anguelov, D.; Erhan, D.; Szegedy, C.; Reed, S.; Fu, C.-Y.; and Berg, A. C. 2016. Ssd: Single shot multibox detector. In *Computer Vision–ECCV 2016: 14th European Conference, Amsterdam, The Netherlands, October 11–14, 2016, Proceedings, Part I 14*, 21–37. Springer.
- Liu, Y.; Qin, Z.; Anwar, S.; Ji, P.; Kim, D.; Caldwell, S.; and Gedeon, T. 2021c. Invertible denoising network: A light solution for real noise removal. In *Proceedings of the IEEE/CVF conference on computer vision and pattern recognition*, 13365–13374.
- Ma, L.; Jin, D.; An, N.; Liu, J.; Fan, X.; and Liu, R. 2023. Bilevel Fast Scene Adaptation for Low-Light Image Enhancement. *arXiv preprint arXiv:2306.01343*.
- Ma, L.; Ma, T.; Xue, X.; Fan, X.; Luo, Z.; and Liu, R. 2022. Practical Exposure Correction: Great Truths Are Always Simple. *arXiv preprint arXiv:2212.14245*.
- Madry, A.; Makelov, A.; Schmidt, L.; Tsipras, D.; and Vladu, A. 2017. Towards deep learning models resistant to adversarial attacks. *arXiv preprint arXiv:1706.06083*.
- Panetta, K.; Gao, C.; and Agaian, S. 2015. Human-visual-system-inspired underwater image quality measures. *IEEE Journal of Oceanic Engineering*, 41(3): 541–551.
- Peng, Y.-T.; Cao, K.; and Cosman, P. C. 2018. Generalization of the dark channel prior for single image restoration. *IEEE Transactions on Image Processing*, 27(6): 2856–2868.
- Piao, Y.; Ji, W.; Li, J.; Zhang, M.; and Lu, H. 2019. Depth-induced multi-scale recurrent attention network for saliency detection. In *Proceedings of the IEEE/CVF international conference on computer vision*, 7254–7263.
- Piao, Y.; Rong, Z.; Zhang, M.; Ren, W.; and Lu, H. 2020. A2dele: Adaptive and attentive depth distiller for efficient RGB-D salient object detection. In *Proceedings of the IEEE/CVF conference on computer vision and pattern recognition*, 9060–9069.
- Prytula, S. 2020. Underwater Object Detection Dataset. <https://public.roboflow.com/object-detection/aquarium>.
- Schroff, F.; Kalenichenko, D.; and Philbin, J. 2015. Facenet: A unified embedding for face recognition and clustering. In *Proceedings of the IEEE conference on computer vision and pattern recognition*, 815–823.
- Su, S.; Yan, Q.; Zhu, Y.; Zhang, C.; Ge, X.; Sun, J.; and Zhang, Y. 2020. Blindly assess image quality in the wild guided by a self-adaptive hyper network. In *Proceedings of the IEEE/CVF Conference on Computer Vision and Pattern Recognition*, 3667–3676.
- Wang, Y.; Li, N.; Li, Z.; Gu, Z.; Zheng, H.; Zheng, B.; and Sun, M. 2018. An imaging-inspired no-reference underwater color image quality assessment metric. *Computers & Electrical Engineering*, 70: 904–913.
- Wang, Z.; Bovik, A. C.; Sheikh, H. R.; and Simoncelli, E. P. 2004. Image quality assessment: from error visibility to structural similarity. *IEEE transactions on image processing*, 13(4): 600–612.
- Wu, J.; Lin, Z.; and Zha, H. 2019. Essential tensor learning for multi-view spectral clustering. *IEEE Transactions on Image Processing*, 28(12): 5910–5922.
- Xiao, M.; Zheng, S.; Liu, C.; Wang, Y.; He, D.; Ke, G.; Bian, J.; Lin, Z.; and Liu, T.-Y. 2020. Invertible image rescaling. In *Computer Vision–ECCV 2020: 16th European Conference, Glasgow, UK, August 23–28, 2020, Proceedings, Part I 16*, 126–144. Springer.
- Xie, C.; Wang, J.; Zhang, Z.; Zhou, Y.; Xie, L.; and Yuille, A. 2017. Adversarial examples for semantic segmentation and object detection. In *Proceedings of the IEEE international conference on computer vision*, 1369–1378.
- Yang, M.; and Sowmya, A. 2015. An underwater color image quality evaluation metric. *IEEE Transactions on Image Processing*, 24(12): 6062–6071.
- Yin, M.; Zhang, Y.; Li, X.; and Wang, S. 2018. When deep fool meets deep prior: Adversarial attack on super-resolution network. In *Proceedings of the 26th ACM international conference on Multimedia*, 1930–1938.
- Yu, Y.; Yang, W.; Tan, Y.-P.; and Kot, A. C. 2022. Towards robust rain removal against adversarial attacks: A comprehensive benchmark analysis and beyond. In *Proceedings of the IEEE/CVF Conference on Computer Vision and Pattern Recognition*, 6013–6022.
- Zhang, M.; Ren, W.; Piao, Y.; Rong, Z.; and Lu, H. 2020. Select, supplement and focus for RGB-D saliency detection. In *Proceedings of the IEEE/CVF conference on computer vision and pattern recognition*, 3472–3481.
- Zhang, S.; Wang, T.; Dong, J.; and Yu, H. 2017. Underwater image enhancement via extended multi-scale Retinex. *Neurocomputing*, 245: 1–9.
- Zhang, W.; Zhuang, P.; Sun, H.-H.; Li, G.; Kwong, S.; and Li, C. 2022. Underwater image enhancement via minimal color loss and locally adaptive contrast enhancement. *IEEE Transactions on Image Processing*, 31: 3997–4010.
- Zhang, Z.; Jiang, Z.; Liu, J.; Fan, X.; and Liu, R. 2023. WaterFlow: Heuristic Normalizing Flow for Underwater Image Enhancement and Beyond. *arXiv:2308.00931*.